Supporting Information

Donges et al. 10.1073/pnas.1117052108

SI Text

Recurrence Network Analysis of Time Series. ***Windowed analysis.*** To detect dynamical transitions in a time series $d(t)$, we view this series through a sliding window of W data points with a step size of ΔW data points. The data within the μ-th window, $x(t) = d(t)|_{t=t_i}$, $i = \mu\Delta W,\ldots,\mu\Delta W + W$, are analyzed separately thereafter. Because of the widely differing average sampling times $\langle\Delta T\rangle$ of all three records (ODP site 659: $\langle\Delta T\rangle_1 = 4.10$ ka, ODP site 721/722: $\langle\Delta T\rangle_2 = 1.81$ ka, ODP site 967: $\langle\Delta T\rangle_3 = 0.36$ ka), and to avoid interpolation, we prescribe the desired average window size W^* in units of time. This approach guarantees that all three records are viewed at a comparable time scale. Our choice of $W^* = 410$ ka is guided by the trade-off between high temporal resolution (small W^*) and statistical confidence (large W^*), but the results are robust within a reasonable range of W^* (1). The windows of $W = \lfloor W^*/\langle\Delta T\rangle \rfloor$ data points then cover approximately W^* years, with deviations of maximum 44% due to irregular sampling. We choose a window overlap of 90%, resulting in a step size of approximately $\Delta W^* = 41$ ka, $\Delta W = \lfloor \Delta W^*/\langle\Delta T\rangle \rfloor$, and maximum deviations of 97%. For every record, the number of data points W in all windows is kept constant (rather than window size in the time domain). Thereby we assure that even extensive statistics (i.e., quantitative measures that do explicitly depend on the number of considered data points) show comparable results along each time series. However, because of the different sampling rates, the choice of a consistent reference time scale W^* for all records requires different choices of W, specifically, $W_1 = 100$ for ODP site 659, $W_2 = 226$ for site 721/722, and $W_3 = 1139$ for site 967, which implies that results from different records should be compared qualitatively only. This limitation does not impact the comparability of the timing of events, because the window lengths all correspond to the reference time scale W^* and we furthermore use the window's midpoints to attach a timing to the recurrence network measures obtained from a particular window (see below).

Embedding of time series. Next, we unfold each time series segment (window) $x(t)$ by time-delay embedding to obtain a vector valued trajectory $\mathbf{x}(t) = \{x(t), x(t+\tau),\ldots,x(t+(m-1)\tau)\}$ (2, 3). The embedding dimension $m = 3$ presents a reasonable compromise given the relatively short time series and the underlying high-dimensional dynamics as suggested by the false nearest neighbor criterion (4, 5). We choose the delay τ to cover approximately the same time scale for all three considered records, i.e., $\tau = \lfloor \tau^*/\langle\Delta T\rangle \rfloor$ with $\tau^* = 10$ ka, corresponding to the order of the decorrelation time for all three time series (1). The result is $\tau_1 = 2$ time steps for ODP site 659, $\tau_2 = 5$ for site 721/722, and $\tau_3 = 27$ for site 967. A detailed discussion of the limitations of this approach with respect to the irregular sampling of the considered time series is given in a complementary technical paper (1).

Recurrence network construction. To represent the recurrence structure within the current time window, we construct an ε-recurrence network (RN) from $\mathbf{x}(t)$ (5–8). The nodes i of this complex network (9, 10) are the W state vectors $\mathbf{x}_i = \mathbf{x}(t = t_i)$ embedded in the m-dimensional reconstructed phase space corresponding to times t_i. We link two nodes i and j if the associated states are very similar—i.e., $\mathbf{x}_i \approx \mathbf{x}_j$. The network's adjacency matrix A_{ij} (9) is given by

$$A_{ij} = \Theta(\varepsilon - \|\mathbf{x}_i - \mathbf{x}_j\|) - \delta_{ij}, \qquad \text{[S1]}$$

where $\Theta(\cdot)$ is the Heaviside function, $\|\cdot\|$ the maximum norm, ε the recurrence threshold, and δ_{ij} the Kronecker delta introduced to exclude self-loops (7). ε is chosen adaptively for each window to guarantee a reasonable choice of the link density fixed at approximately 5% (7, 11). RNs are closely linked with the established concept of recurrence quantification analysis (12), which has been previously used in the context of paleoclimate time series analysis (13, 14).

Network measures and interpretation. So far we have obtained a complex network for each window describing the dust flux dynamics during the associated epoch in the past. We now proceed to quantitatively characterize these networks in terms of two conceptually different graph-theoretic measures (9, 10), which are both sensitive to dynamical transitions in time series mapped to RNs (5, 8, 15). We consider the transitivity properties captured by the measure *network transitivity* (9, 10)

$$\mathcal{T} = \frac{\sum_{i,j,k} A_{ij}A_{jk}A_{ki}}{\sum_{i,j,k} A_{ki}A_{kj}}. \qquad \text{[S2]}$$

$\mathcal{T}$ is larger for regular and smaller for more irregular dynamics within the considered time series segment (5, 8, 15). The *average path length*

$$\mathcal{L} = \langle l_{ij}\rangle_{ij} \qquad \text{[S3]}$$

gives the mean value of the minimum number of links l_{ij} (geodesic graph distance) that have to be crossed to get from node i to j in the RN (9), where $\langle\cdot\rangle_{ij}$ denotes an average over all pairs of nodes. The average is taken only over pairs of nodes that belong to the same network component (i.e., which are mutually reachable on the graph). It tends to fluctuate strongly when the window slides across a dynamical transition (5, 8, 15), because the overall network structure often undergoes a qualitative change at such a point [e.g., because of the merging of two formerly disconnected network clusters (5)].

We use the window's midpoint for plotting the time evolution of $\mathcal{T}$ and $\mathcal{L}$ (see Fig. 2, main text). A notable advantage of our methodology is its insensitivity to changes in the age model underlying $x(t)$. As long as only the time points t_i, but not the actual data $x_i = x(t = t_i)$ (e.g., because of interpolation), differ between age models, our results will remain the same. Note that the only implicit assumption made here is that the available state vectors $\mathbf{x}_i$ in a given time window represent the distribution of states within this window with sufficiently high statistical confidence.

Significance test. Finally, we perform a significance test to ascertain at which times $\mathcal{T}$ and $\mathcal{L}$ deviate significantly from their expected values given the recurrence structure of the whole time series and window size W (8). The corresponding null hypothesis is that the network measures observed for a certain window are consistent with being calculated from a random draw of W state vectors from the prescribed phase space distribution induced by the entire time series. In order to create an appropriate null model, we use the following approach: (*i*) Draw randomly W state vectors from the embedded time series (corresponding to the chosen window size), (*ii*) construct a RN from this set of state vectors, and (*iii*) calculate the network measures of interest.

We obtain a test distribution for each of the network measures and time series separately from 100,000 realizations of this null model. Finally we estimate confidence bands bounded by the test distribution's 5% and 95% quantiles. This simple approach yields a test for stationarity on the basis of the structural features of RNs, where network measures significantly deviating from the empirical test distribution indicate epochs that include potential dynamical regime shifts.

Contemplating Coincidences. ***Introduction.*** We are concerned with the statistical problem of testing for coincidences of two distinct types of events: (*i*) shifts in climate (C events) and (*ii*) the appearance and disappearance of species in the fossil record (S events). Consider a record of N S events $S_1,\ldots,S_N$ and M C events $C_1,\ldots,C_M$ over a time period T, where both sequences are not necessarily ordered chronologically. A single coincidence occurs if an S event falls within the temporal tolerance window of a C event—i.e., $|t_S - t_C| \leq \Delta T$, where t_S and t_C denote the timing of both events (Fig. S1).

Assume that we observe in our record K_e single coincidences. Given these findings and considering the uncertainties in the timing of both types of events as well as the inherent incompleteness of the fossil record, we ask the following questions: Are the observed numbers of coincidences likely to have arisen by pure chance? Can we derive a significance test by combinatorial reasoning?

Statistical null model. Our null hypothesis is that both S and C events are distributed randomly, independently and uniformly over the time interval T. Furthermore, we assume that $\Delta T \ll T/M \ll T$. On the basis of these assumptions, the probability of a specific S event S_i falling into the tolerance window of a specific C event C_j is

$$p = 2\frac{\Delta T}{T}. \qquad \textbf{[S4]}$$

Then the probability of a specific S event S_i coinciding with *at least one* of the M C events is given by

$$1-(1-p)^M = 1-\left(1-2\frac{\Delta T}{T}\right)^M. \qquad \textbf{[S5]}$$

Now we are in a position to compute the probability $P(K;N,1-(1-p)^M)$ that exactly K single coincidences are observed for a given realization of the fully random null model. Because S events are assumed to be distributed independently in the interval $[0,T]$, $P(K;N,1-(1-p)^M)$ is the binomial distribution with N trials and success probability $1-(1-p)^M$ (16) yielding

$$P(K;N,1-(1-p)^M) = \binom{N}{K}\left[1-\left(1-2\frac{\Delta T}{T}\right)^M\right]^K \times \left[\left(1-2\frac{\Delta T}{T}\right)^M\right]^{N-K}. \qquad \textbf{[S6]}$$

From this distribution [Eq. **S6**] we easily derive the expectation value $\langle K\rangle$ and standard deviation $\sigma(K)$ as

$$\langle K\rangle = N[1-(1-p)^M] = N\left[1-\left(1-2\frac{\Delta T}{T}\right)^M\right] \qquad \textbf{[S7]}$$

and

$$\sigma(K) = \sqrt{N[1-(1-p)^M](1-p)^M} = \sqrt{N\left[1-\left(1-2\frac{\Delta T}{T}\right)^M\right]\left(1-2\frac{\Delta T}{T}\right)^M}. \qquad \textbf{[S8]}$$

The p value of an observation K_e with respect to the test distribution [Eq. **S6**]—i.e., the probability to obtain a number of coincidences K larger or equal to the empirically observed number K_e—is then given by

$$P(K \geq K_e) = \sum_{K^*=K_e}^{N} P(K^*;N,1-(1-p)^M). \qquad \textbf{[S9]}$$

Application. Our record of interest spans a time period of $T = 5$ Ma and contains $M = 6$ climate shifts (C events) as well as $N = 2\times 18+1 = 37$ S events (note that *Homo sapiens* is not extinct yet). In Fig. 2 (main text), significant shifts in African climate (C events) are marked by the upper and lower bounds of the gray bars spanning all data and results shown. Coincidences with the time of species appearance and disappearance (S events) considering a temporal tolerance of $\Delta T = 0.1$ Ma are marked by red bars.

The C events occur at approximately 3.5, 2.95, 2.25, 1.6, 1.1, and 0.7 Ma B.P. (Table S1), whereas the timings of all considered S events are listed in Table S2. Given a tolerance $\Delta T = 0.1$ Ma, we observe $K_e = 15$ single coincidences (Fig. 2, main text). This particular choice of the tolerance parameter ΔT is motivated by (*i*) the fact that the timings of most of the considered C and S events have been rounded to the first decimal point prior to the analysis, and (*ii*) uncertainties in dating of the analyzed dust flux records, the detected climate shifts, and hominin fossils which can be assumed to be roughly of this order.

We now aim to quantify the significance of the observed number of coincidences K_e with respect to the null model formulated above—i.e., assuming that both C and S events are distributed uniformly and independently within the time interval of interest. The null model yields an expected number of $\langle K\rangle = 8.04$ coincidences with the standard deviation $\sigma(K) = 2.51$ and the empirical observation corresponding to a p value of $P(K \geq K_e) = 0.003$. The change of p values $P(K \geq K_e)$ and the observed number of coincidences K_e with varying tolerance ΔT is shown in Fig. S2.

Discussion. Our analysis reveals that the observed number of coincidences is robustly significant with p values $P(K \geq K_e) \ll 0.05$ for a range of tolerance parameters $0.05 \leq \Delta T \leq 0.17$ with respect to the fully random null model (Fig. S2*A*). Considerably larger ΔT do not meet the basic assumption $\Delta T \ll T/M \ll T$ any more. In this sense the analysis supports a statement like the following: *The observed coincidences between detected climate shifts and the appearance or disappearance of hominin species are unlikely to arise by chance.* We should emphasize here that coincidence alone, like correlation, does not imply causality (17). It can only serve as a hint at a possible causal relationship.

Note that it is known that the appearance and/or disappearance of different species is typically correlated. This effect is not included in the null model but could be assessed with the help of more sophisticated Monte Carlo simulations. The proposed null model should be seen as the simplest possible quantitative means to justify discussing the influence of Plio-Pleistocene climate change on hominin evolution in the first place.

The presented statistical analysis assumes that the life spans of hominin species are approximated by the times to which their known fossils are dated, an assumption which is also routinely

relied upon in the reconstruction of hominin evolutionary trees or dispersal patterns (18). Minor dating uncertainties and fossil sampling effects are covered by the tolerance parameter ΔT. However, as is always the case in paleontological research, new fossil evidence may dramatically alter the current view of events in hominin evolution summarized in Table S2 (18). Furthermore taphonomic biases and sampling effects may play a significant role (17). Given new evidence, the proposed statistical framework will allow future investigators to quickly evaluate the significance of observed coincidences between C and S events. The same is true if the timing or number of climate shifts were to be revised. Our null model may moreover prove useful to test and compare other hypotheses relating changes in climate to evolutionary events.

Finally it is important to stress that the proposed significance test is asymmetric with respect to C and S events, which is mathematically expressed by the fact that Eq. **S6** is asymmetric with respect to the numbers of events M and N. Above we were concerned with the clustering of S events around C events, thereby implicitly testing for a potential causal influence of C events on S events and *not* vice versa. Considering the research question under study this assumption seems reasonable, because humans are not thought to have had a significant influence on continental and larger scale climate change before a few thousand years ago (see, e.g., the early anthropogenic hypothesis (19)).

1. Donges JF, et al. (2011) Identification of dynamical transitions in marine palaeoclimate records by recurrence network analysis. *Nonlin Processes Geophys* 18:545–562.
2. Packard NH, Crutchfield JP, Farmer JD, Shaw RS (1980) Geometry from a time series. *Phys Rev Lett* 45:712–716.
3. Takens F (1981) in *Dynamical Systems and Turbulence, Warwick 1980*, Lecture Notes in Mathematics, eds Rand D, Young LS (Springer, New York), Vol. 898, pp. 366–381.
4. Kennel M, Brown R, Abarbanel H (1992) Determining embedding dimension for phase-space reconstruction using a geometrical construction. *Phys Rev A* 45:3403–3411.
5. Marwan N, Donges JF, Zou Y, Donner RV, Kurths J (2009) Complex network approach for recurrence analysis of time series. *Phys Lett A* 373:4246–4254.
6. Donner RV, Zou Y, Donges JF, Marwan N, Kurths J (2010) Ambiguities in recurrence-based complex network representations of time series. *Phys Rev E* 81:015101(R).
7. Donner RV, Zou Y, Donges JF, Marwan N, Kurths J (2010) Recurrence networks—A novel paradigm for nonlinear time series analysis. *New J Phys* 12:033025.
8. Donner RV, et al. (2011) Recurrence-based time series analysis by means of complex network methods. *Int J Bifurcat Chaos* 21:1019–1046.
9. Newman M (2003) The structure and function of complex networks. *SIAM Rev* 45:167–256.
10. Boccaletti S, Latora V, Moreno Y, Chavez M, Hwang DU (2006) Complex networks: Structure and dynamics. *Phys Rep* 424:175–308.
11. Schinkel S, Dimigen O, Marwan N (2008) Selection of recurrence threshold for signal detection. *Eur Phys J Spec Top* 164:45–53.
12. Marwan N, Romano MC, Thiel M, Kurths J (2007) Recurrence plots for the analysis of complex systems. *Phys Rep* 438:237–329.
13. Marwan N, Trauth MH, Vuille M, Kurths J (2003) Comparing modern and Pleistocene ENSO-like influences in NW Argentina using nonlinear time series analysis methods. *Climate Dynamics* 21:317–326.
14. Trauth MH, Bookhagen B, Marwan N, Strecker MR (2003) Multiple landslide clusters record Quaternary climate changes in the northwestern Argentine Andes. *Palaeogeogr Palaeoclimatol Palaeoecol* 194:109–121.
15. Zou Y, Donner RV, Donges JF, Marwan N, Kurths J (2010) Identifying complex periodic windows in continuous-time dynamical systems using recurrence-based methods. *Chaos* 20:043130.
16. Jaynes ET, Bretthorst GL (2003) *Probability Theory: The Logic of Science* (Cambridge Univ Press, Cambridge, UK).
17. deMenocal PB (1995) Plio-Pleistocene African climate. *Science* 270:53–59.
18. Strait D, Wood B (1999) Early hominid biogeography. *Proc Natl Acad Sci USA* 96:9196–9200.
19. Ruddiman WF (2007) The early anthropogenic hypothesis: Challenges and responses. *Rev Geophys* 45:RG4001.
20. Trauth MH, et al. (2007) High- and low-latitude forcing of Plio-Pleistocene East African climate and human evolution. *J Hum Evol* 53:475–486.
21. Bromage T, Schrenk F, Zonnefeld F (1995) Paleoanthropology of the Malawi Rift: An early hominid mandible from the Chiwondo Beds, northern Malawi. *J Hum Evol* 28:71–108.
22. Kimbel W, et al. (1996) Late Pliocene Homo and Oldowan tools from the Hadar Formation (Kada Hadar Member), Ethiopia. *J Hum Evol* 31:549–561.
23. Reed K (1997) Early hominid evolution and ecological change through the African Plio-Pleistocene. *J Hum Evol* 32:289–322.
24. White T (2002) in *The Primate Fossil Record*, ed Hartwig W (Cambridge Univ Press, Cambridge, UK), pp. 407–417.
25. Dunsworth H, Walker A (2002) in *The Primate Fossil Record*, ed Hartwig W (Cambridge Univ, Cambridge, UK), pp. 419–436.
26. McHenry H (2002) in *The Primate Fossil Record*, ed Hartwig W (Cambridge Univ Press, Cambridge, UK), pp. 401–406.
27. Antón S, Swisher C (2004) Early dispersals of Homo from Africa. *Ann Rev Anthropol* 33:271–296.
28. White T, et al. (2006) Asa Issie, Aramis and the origin of *Australopithecus*. *Nature* 440:883–889.

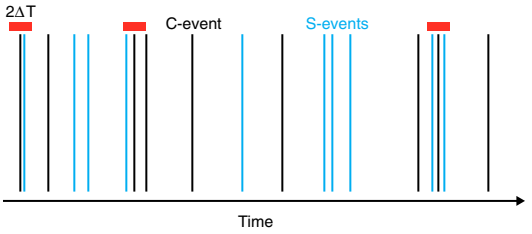

Fig. S1. Schematic representation of C events (black vertical lines) and S events (blue vertical lines). Red horizontal bars of length $2\Delta T$ centered around C events indicate coincidences of one or more S events with one C event. This choice leads to $K_e = 4$ coincidences in this example.

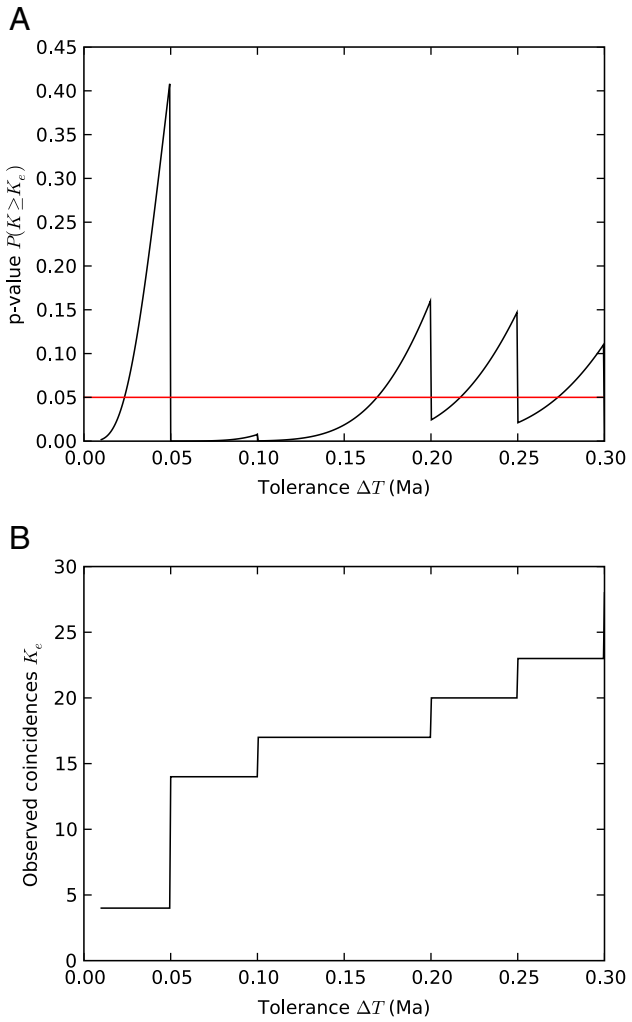

Fig. S2. (*A*) *P* values $P(K \geq K_e)$ of the (*B*) observed number of coincidences K_e for varying tolerance parameter ΔT. We consider the results to be significant if the *p* value is smaller than the commonly chosen significance level of 0.05 (red horizontal line).

Table S1. Timing of climate shifts identified by recurrence network analysis (see main text) and related paleoenvironmental change

Timing, Ma B.P.	Paleoenvironmental change
3.50	Appearance of lakes in EARS
2.95	Disappearance of large lakes in EARS
2.25	Reorganization of Walker circulation (beginning)
1.60	Reorganization of Walker circulation (end)
1.10	Middle Pleistocene transition (beginning)
0.70	Middle Pleistocene transition (end)

EARS, East African Rift System.

Table S2. Times of the appearance and disappearance of hominin species from the known fossil record taken from ref. 20, on the basis of refs. 21–28

Species	Appearance, Ma B.P.	Disappearance, Ma B.P.
Ardipithecus ramidus	4.55	4.40
Australopithecus anamensis	4.20	3.90
Kenyanthropus platyops	3.55	3.45
Australopithecus afarensis	3.60	2.90
Australopithecus bahrelghazali	3.55	3.45
Australopithecus africanus	3.00	2.50
Australopithecus garhi	2.55	2.50
Paranthropus aethiopicus	2.50	2.30
Paranthropus boisei	2.30	1.40
Homo habilis	2.30	1.60
Homo rudolfensis	2.30	1.60
Paranthropus robustus	1.90	1.10
Homo ergaster	1.90	1.00
Homo erectus	1.90	0.30
Homo antecessor	0.90	0.70
Homo heidelbergensis	0.60	0.10
Homo neanderthalensis	0.30	0.05
Homo floresiensis	0.10	0.05
Homo sapiens	0.16	-

The timing of most of these evolutionary S events has been rounded to the first decimal point.